Geol. Mag. **135** (*5*), *1998, pp. 637–655. Printed in the United Kingdom* © *1998 Cambridge University Press*

Relationship between joint spacing and bed thickness in sedimentary rocks: effects of interbed slip

SHAOCHENG JI*, ZHEMING ZHU & ZICHAO WANG

Département de géologie, Université de Montréal, C.P. 6128, Succursale "Centre-Ville", Montréal, Québec, H3C 3J7, Canada

(*Received* 29 April 1997; *revised version received* 2 June 1998; *accepted* 9 June 1998)

Abstract – This paper consists of three parts. The first part presents a critical review of previous mechanical models on the relationship between joint spacing (s) and bed thickness (t) in sedimentary rocks. The second part describes a new mechanical model dealing with the effects of interbed slip on joint spacing. The third part presents the comparison between theoretical results of the model and joint data measured from Cambrian flysch sediments at Plage Victor in the Saint-Jean-Port-Joli area of the Quebec Appalachians. This study demonstrates two formation mechanisms of tensile joints: near-end fracturing takes place in the layers with smaller tensile fracture strength ($C_0 < 30$ MPa) and smaller interbed shear strength ($\tau_0 < 20$ MPa) while mid-point fracturing occurs in those layers with larger C_0 (> 50 MPa) and τ_0 (> 30 MPa) values. For the rocks with moderate tensile fracture strength ($30 < C_0 < 50$ MPa) and interbed shear strength ($20 < \tau_0 < 30$ MPa), the near-end fracturing and mid-point fracturing take place preferentially in the thicker and thinner brittle layers, respectively. In the regime of near-end fracturing, the correlation between s and t is linear and independent of the thickness of the bounding non-jointing layers (d). In the regime of mid-point fracturing, however, the s–t relationship can be either linear or non-linear, depending on the variation of d value. The present study also suggests that the near-end fracturing is probably the prevailing process for the formation of tensile joints in bedded sedimentary rocks and that the coefficient of joint spacing (K) defined by the ratio of s to t is considered as an indicator of $C_0/(2\tau_0)$ for the jointed layer.

1. Introduction

Knowledge of joint spacing is important for the solution of a number of very practical problems in the design and stability of engineering and mining projects, such as major cuts, open pits, as well as large mines and other underground openings and chambers (Price & Cosgrove, 1990). It is also important in the development of models for underground flow of water (Barton & Larsen, 1985; Deloule & Turcotte, 1989; Bear, Tsang & Marsily, 1993) and hydrocarbons (Thunvik & Braester, 1990; Lorenz, Teufel & Warpinski, 1991; Narr & Suppe, 1991) in fractured rocks where a high permeability is so desirable that fractures need to be artificially induced. Knowledge of the rock mass behaviour and permeability is also extremely important for nuclear waste disposal and reservoir construction where it is desirable to prevent leakage. However, it is very difficult for geologists to measure directly the joint spacing in subsurface strata. If a relationship between the joint spacing and bed thickness is known, it is possible for them to determine the joint spacing from the bed thickness data obtained from boreholes.

A linear relationship between median joint spacing and bed thickness has been commonly found in interbedded sediments (Bogdanov, 1947; Novikova, 1947; Kirillova, 1949; Lachenbruch, 1961; Price, 1966; Sowers, 1973; Huang & Angelier, 1989; Aydan & Kawamoto, 1990; Narr & Suppe, 1991; Gross, 1993; Ji & Saruwatari, in press) with a few exceptions (Norris, 1966; Mastella, 1972; Mandal, Deb & Khan, 1994). McQuillan (1973) and Ladeira & Price (1981) reported a linear relationship in beds less than 1.5 m thick and a non-linear relationship in beds up to 12 m thick.

In this paper, we first give a critical review of previous mechanical models on the relationship between joint spacing and bed thickness. Then, we describe a mechanical model that includes the effect of interbed slip on joint spacing in an interbedded sedimentary rock mass. Finally, we compare theoretical results of the model with joint data measured from Cambrian flysch sediments at Plage Victor in the Saint-Jean-Port-Joli area of the Quebec Appalachians.

2. Review of previous works

Three categories of mechanical models (Price, 1966; Hobbs, 1967; Sowers, 1973; Ladeira & Price, 1981; Pollard & Segall, 1987; Mandal, Deb & Khan, 1994; Gross *et al.* 1995; Fischer *et al.* 1995; Ji & Saruwatari, in press) have been proposed to explain the relationship between mean joint spacing and bed thickness. In this section, we will critically review these models.

* Author for correspondence: jish@ere.umontreal.ca

https://doi.org/10.1017/S0016756898001459 Published online by Cambridge University Press

2.a. Shear-lag models

Ramberg (1955), in his paper on boudinage, noted that the tensile stress is built up in a competent layer sandwiched between two incompetent layers due to plastic flow of these incompetent layers. Because the tensile stress increases with increasing area of contact between the contrasting layers, but decreases with increasing cross-section of the competent layer, Ramberg concluded that "the relation between thickness and length of boudins should be such that long boudins are thick and short boudins thin".

Price (1966) reported that field measurements of Bogdanov (1947), Novikova (1947) and Kirillova (1949) indicated an approximately linear relationships between mean joint spacing and bed thickness for two sandstones and a limestone from Russia. Price proposed that the linear relationship between joint spacing and bed thickness is controlled by the transfer of stress from adjacent incompetent beds to the competent layer. The model dealing with the stress transfer is referred to as the shear-lag model in mechanics of composite materials (Cox, 1952; Kelly & Macmillan, 1986).

Hobbs (1967) introduced to geologists the shear-lag model of Cox (1952) and modified the mathematical derivations of the model to incorporate an elastic layer-matrix system. Hobbs' model has two important conclusions. (1) Jointing of a competent layer embedded in a continuous incompetent matrix is a sequential process, and a new joint forms midway between the existing joints because the tensile stress in the competent layer builds up from the ends and reaches the maximum at the centre. (2) The joint spacing (s) is linearly proportional to the bed thickness (t), the square root of the bed's Young's modulus (E_f), and the inverse of the square root of the shear modulus of the matrix (G_m), that is,

$$s = t\sqrt{\frac{E_f}{G_m}}\,\mathrm{cosh}^{-1}\left(\frac{E_f\varepsilon}{E_f\varepsilon - C_0}\right) \qquad (1)$$

(Hobbs' Eq. (16)) where ε is the far-field tensile strain of the layer-matrix system, and C_0 is the tensile strength of the brittle layer. Equation (1) indicates that the joint spacing is influenced by the degree of tectonic deformation (ε).

This equation has been widely cited as a theoretical explanation for the linear relationship between joint spacing and bed thickness in sedimentary rocks (e.g. Price, 1966; McQuillan, 1973; Ladeira & Price, 1981; Huang & Angelier, 1989; Narr & Suppe, 1991; Gross, 1993; Gross *et al.* 1995). However, as pointed out recently by Zhao & Ji (1997), Hobbs' model is based on an assumption that the shear stress in the matrix, which is caused by the strain contrast between the competent layer and the incompetent matrix, decreases linearly from the maximum value at the layer/matrix interface to zero at a distance equal to the jointing layer thickness from the interface (Hobbs' Eq. (9)). This assumption obliges a strict condition that must be met formally for applying Hobbs' model: the incompetent layer thickness should be always larger than the jointing competent layer thickness (Ji & Saruwatari, in press). In many interbedded sedimentary rocks, however, the incompetent layers are very thin relative to jointed layer thickness (Narr & Suppe, 1991; Gross, 1993; Gross *et al.* 1995). Moreover, the shear stress formed by the strain contrast should decrease from the maximum value at the layer/matrix interface to zero at half way between two neighbouring competent layers. In other words, because the layer-matrix composite contains unit-cells which are symmetrically distributed with respect to their boundary, and because the composite is assumed to be deformed by uniform extension, the boundary between two neighbouring unit-cells should be a plane over which no shear stress acts.

In order to eliminate the above shortcomings in the Hobbs' model, Ji & Saruwatari (in press) developed an improved model for the relationship between joint spacing and bed thickness:

$$s = \eta\sqrt{td}, \qquad (2)$$

where

$$\eta = \frac{3}{2}\left[j(1+\upsilon_m)\frac{E_f}{E_m}\right]^{1/2}\mathrm{cosh}^{-1}\left(\frac{E_f\varepsilon}{E_f\varepsilon - C_0}\right). \qquad (3)$$

In Equations (2–3), E_m and υ_m are the Young's modulus and Poisson's ratio of the incompetent layer, respectively; d is the thickness of the bounding non-jointing layers; ε is the tectonic strain, and j is a constant which depends on the decay mode of shear stress in the incompetent layers. Equations (2) and (3) suggest that joints form only when the layer-parallel extensional strain $\varepsilon \geq C_0/E_f$ and that increasing amounts of ε result in a decrease in joint spacing (Fig. 1). As shown in Figure 1a, the ε–s curve displays an initial rapid, non-linear decrease in joint spacing at low extensional strains followed by an apparent steady state at large extensional strains. The transition between these two regimes occurs after a certain threshold strain is achieved. Below this critical strain (between lines AB and CD in Fig. 1b), joints develop through sequential fracturing. Above the critical strain, however, joint spacing stops evolving and remains nearly constant. This regime (on the left-hand side of line CD in Fig. 1b) is inferred as 'fracture saturation' by Rives *et al.* (1992) and Wu & Pollard (1992, 1995). On the right-hand side of line AB in Figure 1b, $\varepsilon < C_0/E_f$ and no fracturing takes place.

Equations (2) and (3) show that joint spacing depends not only on the Young's modulus, tensile strength and thickness of the jointing layer, but also on the Young's modulus, Poisson's ratio and thickness of the bounding non-jointing layers. Interestingly,

https://doi.org/10.1017/S0016756898001459 Published online by Cambridge University Press

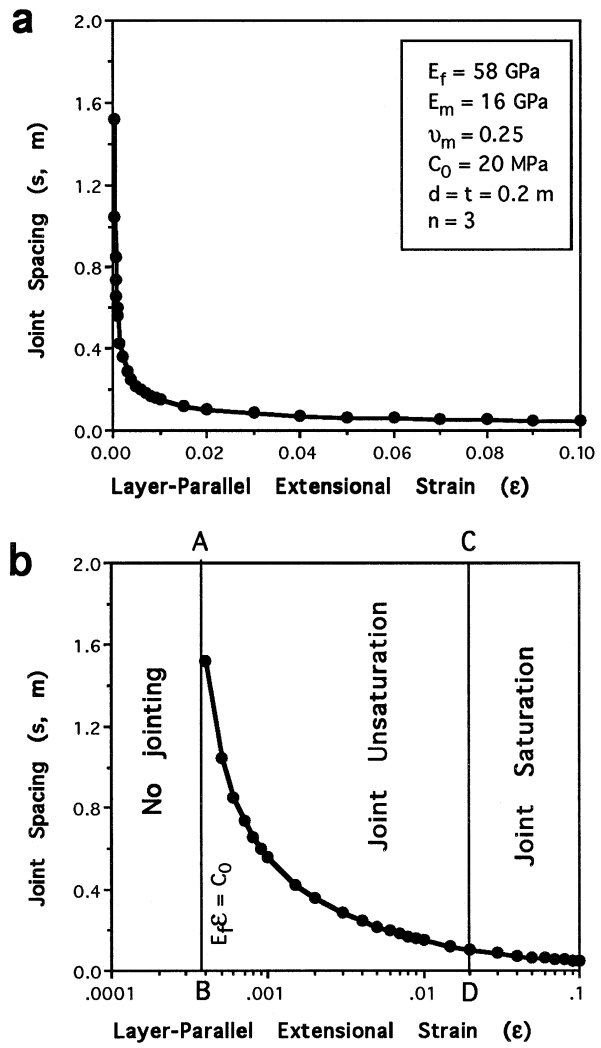


Figure 1. Relationship between joint spacing and applied layer-parallel extensional strain, predicted by a revised shear-lag model (Ji & Saruwatari, in press). The model assumes that the interfaces between competent and incompetent layers are welded. Model parameters: E_f=58 GPa, E_m=16 GPa, υ_m=0.25, C_0=20 MPa, $d=t$=0.2 m, and n=3. 'Fracture saturation' occurs after the applied strain is larger than 0.01. Data are represented in a linear scale (a) and in a logarithmic scale (b).

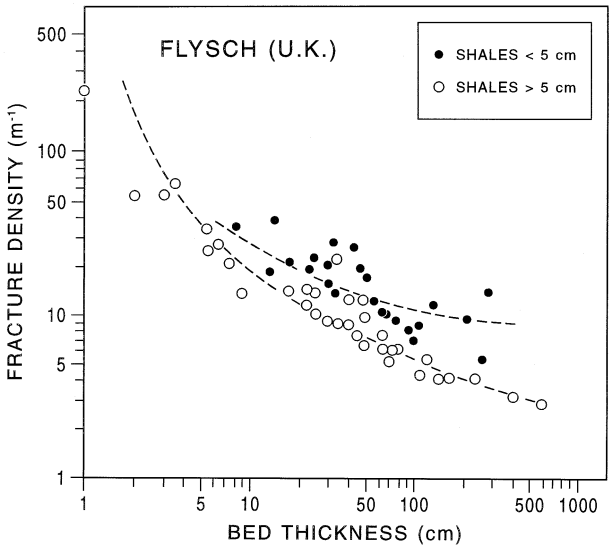


Figure 2. Relationship between fracture density and competent bed thickness for different thickness of adjacent incompetent layers in the Carboniferous flysch of Devon and Cornwall (UK). The fracture density is defined as the number of fractures per metre. The fracture density in the competent layers which adjoin incompetent shale layers thicker than 5 cm is significantly smaller (for a given thickness of competent layer) than when the adjacent shale layers are thinner than 5 cm. After Ladeira & Price (1981).

Equation (2) predicts that the joint spacing, for a given thickness of competent layer, increases with an increase in the thickness of adjacent incompetent layers. As shown in Figure 2 (Ladeira & Price, 1981), the joint spacing in the competent layers which adjoin incompetent layers thicker than 5 cm is significantly larger (for a given thickness of competent layer) than when the adjacent layers are thinner than 5 cm. This indicates that the development of joints in the competent beds is also related to the thickness of the adjacent layers of incompetent material.

Moreover, Equation (2) suggests that the relationship between s and t is linear if the ratio of t to d is constant. If d is constant or (d–t) is constant, the mean joint spacing increases as a function of the square root of the bed thickness, that is, $s \propto \sqrt{t}$. Mandal, Deb & Khan (1994) carried out a series of experiments using rigid layers of plaster of Paris with different thicknesses resting on a ductile substratum of pitch with a constant thickness. They observed that the mean joint spacing is proportional to the square root of the bed thickness. Hence the relationship between s and t depends on the relationship between t and d.

Sowers (1973) developed a model to explain joint spacing based on the idea that stress concentrations develop at periodic instabilities that are initiated at the interface between lithological layers with contrasted elastic properties. His model also predicted that the joint spacing increases linearly with thickness of the jointed layer. However, his calculations show that an extremely high longitudinal strain is needed to create even very low joint density. As pointed out by Narr & Suppe (1991), if Sowers' model has any applicability to natural fractures it is probably to brittle boudins enclosed in a viscous matrix, but not to joints.

McQuillan (1973) and Ladeira & Price (1981) reported that joint spacing in beds thicker than 1.5 m shows a non-linear relationship with bed thickness, whereas joint spacing in those thinner than 1.5 m shows a linear relationship. Ladeira & Price (1981) assumed that these different relationships correspond to different mechanisms: spacing in thin layers is influenced by the shear-lag effect at the competent–incompetent rock interfaces, whereas spacing in thick layers is independent of bed thickness and results from an

https://doi.org/10.1017/S0016756898001459 Published online by Cambridge University Press

hydraulic fracture mechanism. The hypothesis proposed by Ladeira & Price (1981) is still doubtful for the following reasons. (1) The joints are generally accepted to have been formed in the upper crust shallower than a few kilometres, where there is good permeability due to the high connectivity of fluid-migration pathways along linked pores and interfaces between layers. In such an environment, the fluid pressure should remain near-hydrostatic (e.g. Reynolds & Lister, 1987). (2) Most of the joints observed in the field are not filled with hydrothermal vein materials such as calcite or quartz. (3) The model of Ladeira & Price (1981) predicts an increase in fracture spacing with increasing permeability of the unfractured rock. If this were true, one would expect fractures in porous, coarse-grained sandstones (with high permeability) to be more widely spaced than in massive limestones (with low permeability). Field data from McQuillan (1973) and Ladeira & Price (1981) do not support the above prediction.

Mandal, Deb & Khan (1994) analysed the spacing of tensile fractures in a strong brittle layer encased in weak viscous matrix. Their analyses may be more appropriate for boudins whose gaps are filled with flowing matrix material than for most joints which are not filled at all (barren fractures or free surfaces). Based on an audacious assumption described by their Equation (6), they obtained the following relationship between joint spacing and bed thickness:

$$s = \left[\left(\frac{C_0}{\eta^{1-k}}\right)\left(\frac{t}{\dot{\varepsilon}}\right)\right]^{1/2} \tag{4}$$

where η is the matrix viscosity, k is an arbitrary positive constant (Mandal, Deb & Khan, 1994), and $\dot{\varepsilon}$ is the far-field longitudinal strain-rate parallel to the layering. Equation (4) implies that the competent layer has a unit of length in the direction perpendicular to the extension and in the layering plane. It is easy to note that Equation (4) is correct only when $k=0$.

Equation (4) can be rewritten as

$$s = \left(\frac{C_0}{\sigma_m}\frac{\dot{\varepsilon}_m}{\dot{\varepsilon}}t\right)^{1/2} \tag{5}$$

for $k=0$, where $\dot{\varepsilon}$ and $\dot{\varepsilon}_m$ are the far-field longitudinal strain-rate of the layer-matrix system and the matrix strain-rate, respectively, and σ_m is the mean tensile stress of the matrix. Since $\dot{\varepsilon}_m/\dot{\varepsilon} \geq 1$ and $C_o/\sigma_m \geq 1$, the joint spacing s should be always larger than $\sqrt{t}$. However, Ladeira & Price (1981) reported that in a greywacke from the Carboniferous flysch of Devon and Cornwall (UK), the mean joint spacing is smaller than the square root of the bed thickness. Clearly, this cannot be predicted by the model of Mandal, Deb & Khan (1994). In addition, the volume fraction of brittle layer is not a parameter in the mechanical model of Mandal, Deb & Khan (1994). Such a treatment implies that the fracture spacing does not depend on the thickness of the non-jointing weak layer between two competent layers. This does not agree with the field data reported by Ladeira & Price (1981, Fig. 2).

2.b. Stress-perturbation models

This category of models (Lachenbruch, 1961; Pollard & Segall, 1987; Fischer *et al.* 1995; Gross *et al.* 1995) considers that joints are free surfaces, and consequently the joint-normal tensile stress in the vicinity of a joint is locally reduced with respect to the far-field tensile stress. This stress reduction prevents the formation of new joints in the vicinity of existing joints. The region of reduced stress, referred to as 'stress reduction shadow' by Gross *et al.* (1995) and Becker & Gross (1996), scales with joint height. The size of the stress reduction shadow controls joint spacing.

Pollard & Segall (1987) found that the magnitude of local stress normal to the joint surface (σ_{11}) at a distance away from the joint (the width of so-called shadow zone) in a homogeneous, infinite elastic medium is a function of distance from the joint (x) and mechanical layer thickness (t):

$$\sigma_{11} = 8\sigma^*\left(\frac{x}{t}\right)^3\left[4\left(\frac{x}{t}\right)^2+1\right]^{-3/2} \tag{6}$$

where σ^* is the far-field stress, that is, $\sigma^*=E\varepsilon$, where E and ε are Young's modulus and the far-field strain of the rock. If σ_{11} is higher or equal to the tensile strength (C_0) of the layer then the layer will fracture. Thus, the theoretical model of Pollard & Segall (1987) gave a linear relationship between s and t:

$$s = \frac{t}{2}\left[\left(\frac{E\varepsilon}{C_0}\right)^{2/3}-1\right]^{-1/2}. \tag{7}$$

The following points deserve to be mentioned. (1) Since this model considered only an infinite elastic medium without layered structure, it can be applied to homogeneous rock masses such as granites and massive thick-bedded carbonates where joints terminate at random locations. The model cannot be applied to sedimentary sequences which consist of different mechanical layers. In the well-bedded sedimentary masses, joints terminate consistently at mechanical layer boundaries (e.g. Gross, 1993). (2) This model predicts that new joints occur in the vicinity of existing joints. Thus, mid-point fracturing (Hobbs, 1967; Masuda & Kuriyama, 1988; Ji & Zhao, 1993) cannot be predicted by this model. (3) This model implies that the far-field tensile stress ($\sigma^*=E\varepsilon$) always exceeds the tensile strength (C_0) of the rock mass since Equation (6) is valid only for $E\varepsilon > C_0$.

Recently, Gross *et al.* (1995) conducted finite element numerical simulations for the two-dimensional

https://doi.org/10.1017/S0016756898001459 Published online by Cambridge University Press

stress distribution around a crack confined to one layer of a layered elastic medium under far-field extension. They observed that lateral extent of the stress reduction shadow created by a pre-existing joint increases with height of this joint, which corresponds to bed thickness for many layered sedimentary rocks. They concluded that the linear correlation between joint spacing and bed thickness commonly observed in outcrop is a direct result of this relationship. In addition, their theoretical results showed that the size of the stress reduction shadow increases significantly with increasing E_f/G_m, implying that joint spacing should be greater in stiffer beds. This result is in agreement with the numerical solution of Fischer *et al.* (1995) and analytical solution of Hobbs (1967). However, in nature, joint spacing is often closer in stiffer beds. Gross *et al.* (1995) interpreted this contradiction as due to the fact that beds with higher Young's moduli fail at lower magnitudes of extensional strain.

Finite-element analysis of Fischer *et al.* (1995) demonstrated that there is no clear relationship between joint spacing and bounding unjointed bed thickness. However, their result is inconsistent with field observations of Ladeira & Price (1981). Fischer *et al.* (1995) attributed the above discrepancy to the boundary conditions employed in their model. Their model assumes perfectly bonded interfaces while interbed slip takes place in natural sedimentary rocks.

Obviously, the shear-lag models are different from the stress-perturbation models in the following respects. First, the shear-lag models consider that the far-field tensile stress is always smaller than the tensile strength of the jointing rock layer and is equal to the elastic or flow stress of the incompetent layers because stresses cannot be transmitted across free surfaces such as open cracks. Second, the shear-lag models consider that the tensile stress is concentrated in the strong layer due to the stress transfer from the adjacent incompetent layers, the concentrated stress can be locally and temporally equal to the tensile fracture strength of the jointing layer and results in formation of joints. The magnitude of the stress concentration depends on mechanical properties and thicknesses of both competent and incompetent layers and far-field strain.

2.c. Energy balance model

Taking into account the total energy dissipated by the elastic deformation–brittle fracture process, Souffaché & Angelier (1989) obtained the following relationship between the spacing (s) and layer thickness (t):

$$s = \frac{2\pi C_0^{\,2}}{\upsilon\rho g E} \cdot \frac{t}{t + t_c} \tag{8}$$

where E, υ, ρ and C_0 are the Young's modulus, Poisson's ratio, rock density and tensile fracture strength of the competent layer; g is the acceleration due to gravity; and t_c is a critical thickness which is given by

$$t_c = \frac{2\left[\sigma_0 - (1-2\upsilon)P + \upsilon\rho' gH\right]}{\upsilon\rho g}. \tag{9}$$

In Equation (9), σ_0 is the residual tensile stress induced by friction with adjacent beds after rupture has occurred, P is the hydrostatic pore pressure, ρ' is the rock density of the overlying terranes and H is the burial depth of the layer. Equation (8) implies that the joint spacing is linearly proportional to bed thickness for thin layers ($t << t_c$), and becomes constant for thick layers ($t >> t_c$)). Angelier *et al.* (1989) used this model to explain variations of joint spacing as a function of bed thickness in sandstone and limestone of the Colorado Plateau. However, mechanical properties of the incompetent layers were not incorporated into Equation (8). The mechanical properties should influence the magnitude of the stresses transferred from the incompetent layers to the jointing competent layer.

2.d. Summary

Although each of the models mentioned above has contributed to progress in the mechanical analysis of joint spacing, an obvious problem is that they have ignored the effects of possible slip on the bed interfaces. All the previous models assumed that bedding interfaces are perfectly bonded so that there is no slip between the layers. In the following section, we will discuss the effect of the interface sliding on the joint spacing.

3. Effects of interbed sliding

In the unit cell shown in Figure 3, a jointed competent layer lies between two incompetent (matrix) beds, with joints forming the ends of the layer (AB and CD planes in Fig. 3). Because joints are free surfaces across which no stress can be transferred (Lachenbruch, 1961; Pollard & Segall, 1987), the far-field extensional strain (ε) cannot be directly applied to a discontinuous, jointed layer segment (ACDB in Fig. 3) from its ends (AB and CD planes in Fig. 3). Thus, the tensile stress built-up in this layer segment is purely due to the stress transfer from the matrix to the competent layer by means of interfacial shear stresses (Hobbs, 1967). In the following mechanical analysis, we will use the shear-lag model developed by Cox (1952) and summarized by Piggott (1980) and Kelly & Macmillan (1986). This model has been widely used by material scientists to predict elastic strength of two-phase composites (e.g. Nardone & Prewo, 1986; Ji & Zhao, 1994; Zhao & Ji, 1992, 1997).

If the interface transfers the stress from the weak matrix to the strong layer with no slip, the tensile stress

https://doi.org/10.1017/S0016756898001459 Published online by Cambridge University Press

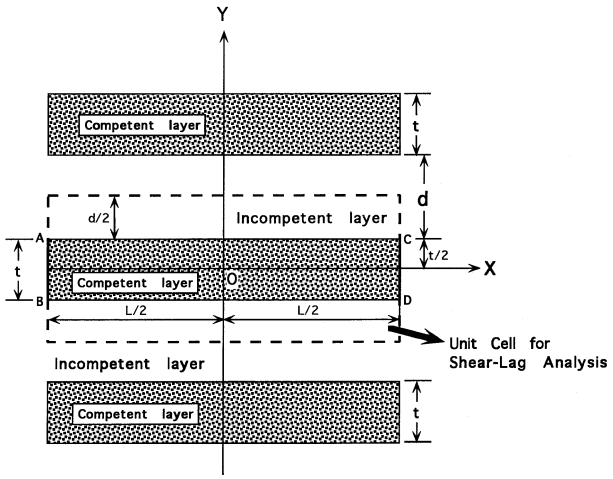


Figure 3. Schematic illustration of the mechanical equilibrium analysis in the shear-lag model for the layer-matrix system. Variables are defined in text.

in the layer [$\sigma_f(x)$] and the shear stress at the layer/matrix interface [$\tau(x,t/2)$] can be calculated, respectively, according to the following equations:

$$\sigma_f(x) = E_f \varepsilon \left(1 - \frac{\cosh(\beta x)}{\cosh\left(\frac{\beta L}{2}\right)}\right) \tag{10}$$

and

$$\tau(x,t/2) = \frac{t}{2} E_f \varepsilon \beta \frac{\sinh(\beta x)}{\cosh\left(\frac{\beta L}{2}\right)} \tag{11}$$

where L is the original joint spacing (Fig. 3), E_f and t are the Young's modulus and the thickness of the competent layer, respectively, and

$$\beta = \left(\frac{8G_m}{E_f t d}\right)^{1/2} \tag{12}$$

where G_m and d are the shear modulus and the thickness of the incompetent layer (that is, matrix), respectively. Equation (12) is based on an assumption that the shear stress formed by the strain contrast between the layers decreases linearly with increasing the vertical distance (Hobbs, 1967) from the maximum value $\tau(x,t/2)$ at the bedding interface to zero midway between two neighbouring competent layers. This assumption will make mathematical treatments simple, although the actual shear stress may decrease nonlinearly in the Y direction (Fischer *et al.* 1995; Ji & Saruwatari, in press).

As shown schematically in Figure 4d, the tensile stress in a competent layer builds up from the ends ($x = \pm L/2$) and has the maximum at the centre ($x = 0$). In contrast, the layer/matrix interfacial stress has a maximum at the layer ends ($x = \pm L/2$) and a minimum at the centre of the layer ($x = 0$).

If the interfacial shear stress reaches the shear strength of the interface (τ_0), slip will occur over a length $0.5L_s$ at both ends of the competent layer segment (Fig. 4e). Here L_s is the total length of the slipped interface rather than any displacement across the interface. Once the slip takes place, the interfacial shear stress for the slipping parts is constant and equal to the shear strength of the interface (τ_0). For the central part of the competent layer, there is no interfacial slip since the interfacial shear stress is still lower than τ_0, and controlled by the shear-lag effect (Fig. 4c, e). Thus, the layer end and centre regions should be treated separately.

In the case where the incompetent layers are ductile, the shear stress is also constant in the slip regions shown in Figure 4e, and equal to the shear yield stress of the incompetent layer, if we neglect work hardening and the adhesion between layers is perfect.

The shear-lag model (Cox, 1952; Piggott, 1980; Kelly & Macmillan, 1986) assumes that the soft matrix as a whole is strained homogeneously, but locally the state of uniform stress and strain is perturbed by transfer of stress to the strong layer (Fig. 4). If there is no slipping along the interfaces between the competent and incompetent layers and $P(x)$ is the load in the competent layer, Cox (1952) assumed

$$\frac{dP(x)}{dx} = H\left[u(x) - v(x)\right] \tag{13}$$

where $u(x)$ is the longitudinal displacement in the layer and $v(x)$ is the corresponding displacement the matrix would undergo if the competent layer were absent; H is a constant, the value of which depends on the geometrical arrangement of the layers and matrix and on their respective elastic moduli.

In the regime of elastic deformation, according to the Hooke's law, the load in the layer is:

$$P(x) = E_f A_f \frac{du(x)}{dx} \tag{14}$$

where E_f is Young's modulus, and A_f is the area of cross-section of the competent layer. $A_f = bt$, where t and b are the thickness and width of the competent layer in the Y and Z directions (Fig. 3), respectively.

Differentiating Equation (13) and substituting Equation (14) gives

$$\frac{d^2P}{dx^2} = H\left(\frac{P}{E_f A_f} - \varepsilon\right) \tag{15}$$

where $\varepsilon = dv(x)/dx$. This differential equation is solved as

$$P(x) = E_f A_f \varepsilon + S_1 \sinh(\beta x) + S_2 \cosh(\beta x) \tag{16}$$

https://doi.org/10.1017/S0016756898001459 Published online by Cambridge University Press

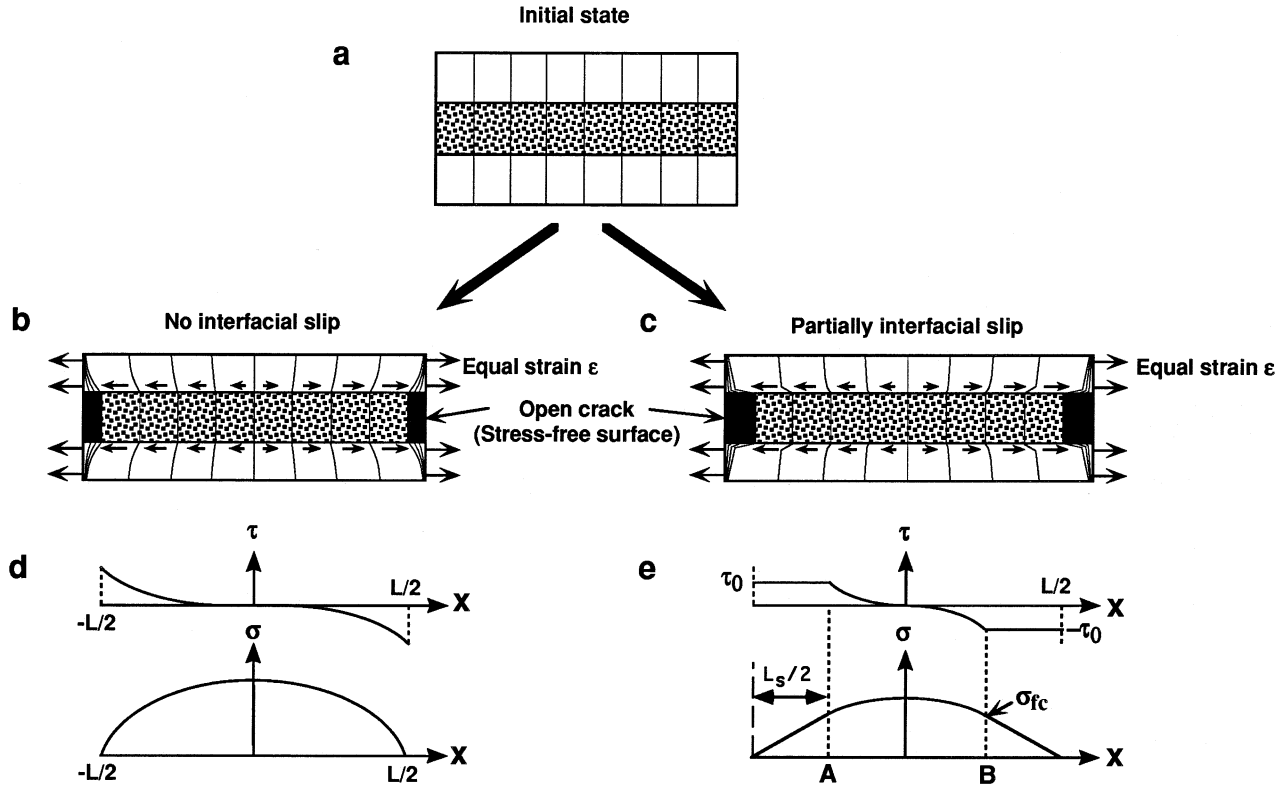


Figure 4. Schematic illustration of the differences between two mechanical models. (a) Unstressed layer-matrix system. (b) and (c) Stressed layer-matrix systems. These figures show the variations of the longitudinal displacements introduced by applying a uniform extensional strain at the ends of the matrix. The openings at joints are exaggerated. No slip takes place at the layer/matrix interfaces in (b). In (c), slip occurs over a length of $L_s/2$ at both ends of the layer whereas near the layer mid-part no slip takes place at the layer/matrix interfaces. (d) and (e) Distributions of the interfacial shear stress and tensile stress for the competent layers with no interbed slip (d) and with partially interbed slip (e). At the slipping interfaces, the shear stress is equal to the interbed shear strength (τ_0). The interbed slip decreases the maximum tensile stress within the competent layer.

or

$$\sigma_f(x)=\frac{P(x)}{A_f}=E_f\varepsilon+\frac{S_1}{A_f}\sinh(\beta x)+\frac{S_2}{A_f}\cosh(\beta x) \quad (17)$$

where

$$\beta=\left(\frac{H}{E_f A_f}\right)^{1/2}=\left(\frac{8G_m}{E_f t d}\right)^{1/2} \quad (18)$$

and S_1 and S_2 are constants which can be determined according to the following boundary conditions:

$$\sigma_f=\sigma_{fc} \text{ at } x=\pm(L-L_s)/2 \quad (19)$$

for the central part of the competent layer. σ_{fc} is the maximum stress transferred to the competent layer in the slip regions (Fig. 4e) and will be determined later. Insertion of these boundary conditions into Equation (17) gives

$$S_1=0, \quad (20)$$

$$S_2=\frac{A_f(\sigma_{fc}-E_f\varepsilon)}{\cosh[\beta(L-L_s)/2]}. \quad (21)$$

and thus

$$\sigma_{fe}(x)=E_f\varepsilon+(\sigma_{fc}-E_f\varepsilon)\frac{\cosh(\beta x)}{\cosh[\beta(L-L_s)/2]} \quad (22)$$

where $\sigma_{fe}(x)$ is the internal tensile stress in the centre region of the layer.

The elastic contribution to the layer stress is determined by the magnitude of the maximum interfacial shear stress. The highest shears are at the boundaries of the elastic stress transfer region [$x=\pm(L-L_s)/2$] and are equal to the shear strength of the interface (τ_0) (Fig. 4e). We proceed as follows. Differentiating Equation (22), we obtain

$$\frac{d\sigma_{fe}(x)}{dx}=(\sigma_{fc}-E_f\varepsilon)\beta\frac{\sinh(\beta x)}{\cosh[\beta(L-L_s)/2]}. \quad (23)$$

If $\tau(x,y)$ is the shear stress, in the x direction, on planes parallel to this direction (Fig. 3), then, at the interface between the layer and the matrix, the shear stress is $\tau(x,t/2)$. According to mechanical equilibrium, we have

$$dP(x)=-2\tau(x,t/2)(b dx). \quad (24)$$

From Equation (24), we can obtain the shear stress at the layer/matrix interface ($y=t/2$):

https://doi.org/10.1017/S0016756898001459 Published online by Cambridge University Press

$$\tau(x,t/2) = -\frac{1}{2b}\frac{dP(x)}{dx} = -\frac{A_f}{2b}\frac{d\sigma_{fe}(x)}{dx} = -\frac{t}{2}\frac{d\sigma_{fe}(x)}{dx} \quad (25)$$

because $A_f = bt$.

Substituting Equation (23) into Equation (25) and considering the boundary conditions $\tau = \tau_0$ at $x = \pm(L-L_s)/2$, we obtain the layer internal tensile stress in the non-slip region:

$$\sigma_{fc} = E_f\varepsilon - \frac{2\tau_0}{t\beta}\frac{1}{\tanh[\beta(L-L_s)/2]}. \quad (26)$$

We now turn to the layer ends. Here the interfacial shear stress is constant at $\tau = \tau_0$ (Fig. 4e), thus from Equation (25) we have

$$\tau_0 = -\frac{t}{2}\frac{d\sigma_{fs}(x)}{dx} \quad (27)$$

where $\sigma_{fs}(x)$ denotes the layer internal tensile stress in the slip region. Integrating Equation (27) with the boundary conditions $\sigma_{fs} = 0$ at $x = L/2$, we find

$$\sigma_{fs}(x) = \frac{2}{t}\tau_0\left(\frac{L}{2} - x\right) \quad (28)$$

Since $\sigma_{fs}(x) = \sigma_{fc}$ at $x = (L-L_s)/2$ (Fig. 4e),

$$\sigma_{fc} = \frac{L_s}{t}\tau_0. \quad (29)$$

Eliminating σ_{fc} between equations (26) and (29), we obtain

$$L_s = \frac{E_f\varepsilon t}{\tau_0} - \frac{2}{\beta}\frac{1}{\tanh[\beta(L-L_s)/2]} \quad (30)$$

or

$$L_s = \frac{E_f\varepsilon t}{\tau_0} - \frac{\sqrt{\frac{E_f td}{2G_m}}}{\tanh\left[(L-L_s)\sqrt{\frac{2G_m}{E_f td}}\right]}. \quad (31)$$

This is a transcendental equation which can be solved using the Newton-Raphson method (Kreyszig, 1993). A FORTRAN program for solving Equation (31) is available upon request from the first author.

Figure 5 shows the variations of sliding interface length (L_s) as a function of fractured layer length (L) and thickness (t) and the soft layer thickness (d). In the calculations, the parameters used are: $E_f = 58$ GPa, $G_m = 7.74$ GPa, $\tau_0 = 10.00$ MPa, and $\varepsilon = 1.12\times10^{-3}$. In the case where $d = t$ (Fig. 5a), the relationship between L_s and t becomes linear as long as $L/t \geq 10$. This is because when

$$(L-L_s)\sqrt{\frac{2G_m}{E_f td}} \geq 2.60, \quad (32)$$

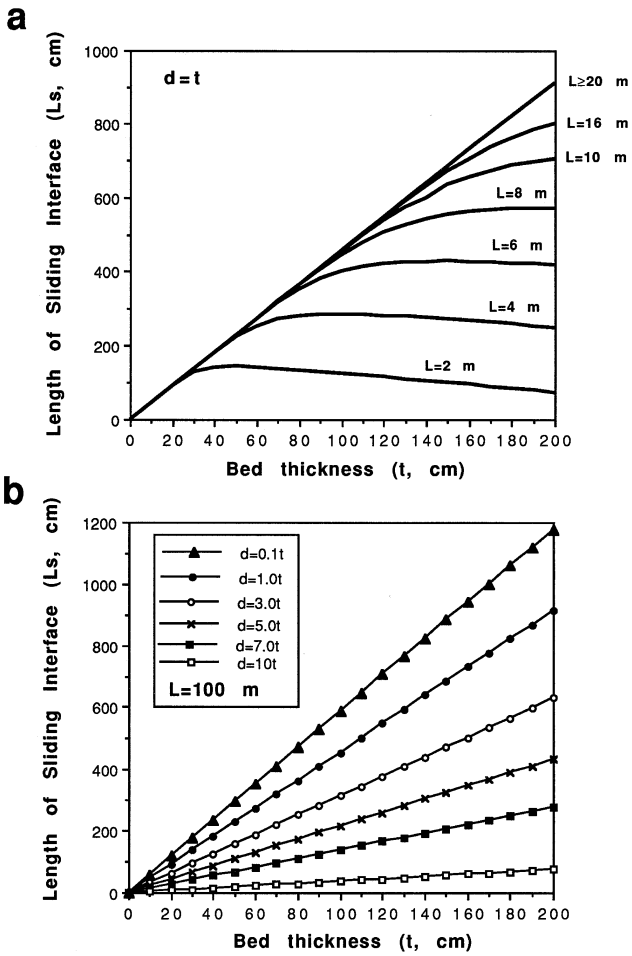


Figure 5. Variations of sliding interface length (L_s) as a function of fractured layer length (L), thickness (t) and the bounding non-jointed layer thickness (d). Model parameters: $E_f = 58$ GPa, $G_m = 7.74$ GPa, $\tau_0 = 10$ MPa, and $\varepsilon = 1.12\times10^{-3}$. $d = t$ for (a) and $d = kt$ for (b), where k is a constant. The k value varies from 0.1 to 10 in (b).

$$\tanh\left[(L-L_s)\sqrt{\frac{2G_m}{E_f td}}\right] \approx 1 \quad (33)$$

with better than 1% accuracy. Figure 5b shows that there is a linear relationship between L_s and t for $L/t \geq 50$, and that the sliding interface length L_s increases with decreasing the d/t ratio.

Substituting equation (29) into equation (23), we have

$$\sigma_{fe}(x) = E_f\varepsilon - \left(E_f\varepsilon - \frac{L_s}{t}\tau_0\right)\frac{\cosh(\beta x)}{\cosh[\beta(L-L_s)/2]}. \quad (34)$$

Because $\left(E_f\varepsilon - \frac{L_s}{t}\tau_0\right)$ is always larger than 0, the maximum tensile stress in the layer $[(\sigma_{fe})_{max}]$ occurs at $x = 0$ (Fig. 4e) and is given by

https://doi.org/10.1017/S0016756898001459 Published online by Cambridge University Press

$$\sigma_{fe}(x)_{\max} = E_f\varepsilon + \frac{\left(\frac{L_s}{t}\tau_0 - E_f\varepsilon\right)}{\cosh\left[\beta\left(L-L_s\right)/2\right]}. \qquad (35)$$

When the magnitude of the maximum tensile stress reaches the tensile fracture strength (C_0) of the layer, a new joint forms midway between the existing joints, and tensile stress goes to zero at this point. The critical length of the layer segment possible below which the maximum tensile stress cannot exceed the fracture strength is thus determined by the following equation:

$$L_c = L_s + \frac{2}{\beta}\cosh^{-1}\left(\frac{E_f\varepsilon - \frac{L_s}{t}\tau_0}{E_f\varepsilon - C_0}\right). \qquad (36)$$

L_c is the shortest length of layer segment which can fracture because in shorter segments the tensile stress nowhere exceeds the tensile strength of the layer. Segments longer than L_c, however, will fracture again. The minimum length of the layer segment possible should be equal to $L_c/2$ because segments shorter than L_c cannot fracture further. Therefore, according to Ohsawa *et al.* (1978), there is a range of layer segment lengths: $L_c/2 \le L_j \le L_c$, where L_j is the length of jointed layer segments. If the frequency distribution of fracture spacing is a normal distribution in the range from $L_c/2$ to L_c, Ohsawa *et al.* (1978) suggest the mean fracture spacing (s) to be:

$$s = \frac{3}{4}L_c, \qquad (37)$$

that is,

$$s = \frac{3}{4}L_s + \frac{3}{2\beta}\cosh^{-1}\left(\frac{E_f\varepsilon - \frac{L_s}{t}\tau_0}{E_f\varepsilon - C_0}\right) \qquad (38)$$

where L_s is given by Equation (30).

From Equations (22) and (31), the centre part shear stress (τ_e) on the layer/matrix interfaces can be determined according to

$$\tau_e = \frac{1}{2}\left(E_f\varepsilon t - L_s\tau_0\right)\beta\frac{\sin(\beta x)}{\cosh\left[\beta\left(L-L_s\right)/2\right]}. \qquad (39)$$

Figure 6 shows an example of the calculation of the layer internal tensile stress (Fig. 6a) and the layer/matrix interfacial shear stress (Fig. 6b) using equations (28), (34) and (39). The mechanical parameters used in the calculations are the following: $E_f = 58$ GPa, $G_m = 7.74$ GPa, $\tau_0 = 10$ MPa, $C_0 = 20.00$ MPa and $\varepsilon = 1.12\times10^{-3}$. Clearly, stress distribution curves (Fig. 6a, b) consist of two parts. The centre part is governed by the shear-lag effect or elastic stress transfer, and the end parts are controlled by the slip on the layer/matrix

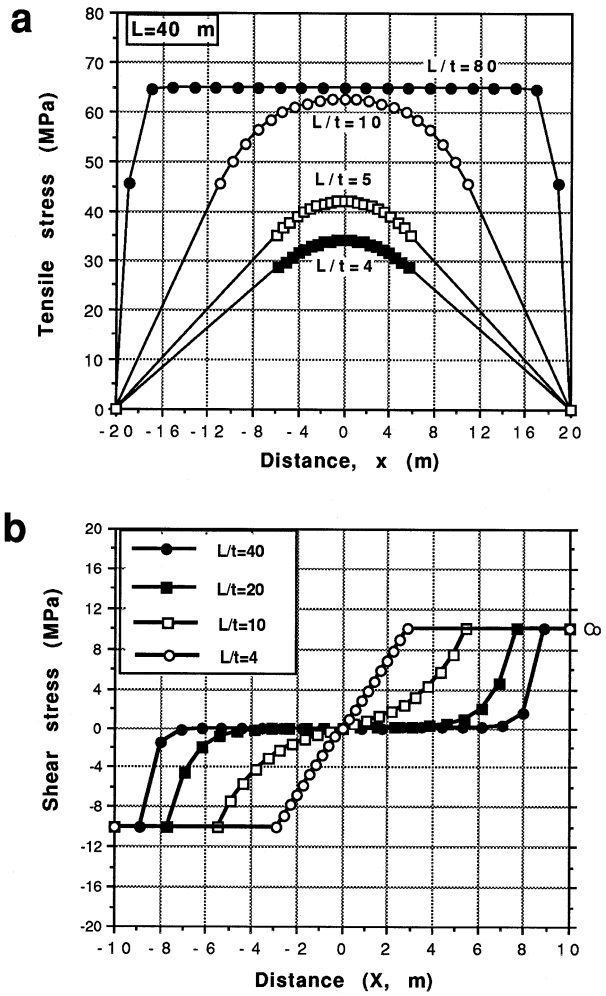


Figure 6. Variations of the layer internal tensile stress (a) and the layer/matrix interfacial shear stress (b) as a function of the length/thickness (L/t), along the layer. Model parameters: $E_f = 58$ GPa, $G_m = 7.74$ GPa, $\tau_0 = 10$ MPa, and $\varepsilon = 1.12\times10^{-3}$, and $d = t$. $L = 40$ m for (a) and $L = 20$ m for (b).

interfaces. Figure 6 also indicates that the sliding interface length (L_s) depends on the initial ratio of the layer length to the thickness (L/t). The L_s value increases with decreasing the L/t ratio.

Equation (39) predicts a mid-point fracturing process for the brittle layer because the maximum tensile stress occurs at the centre of the layer (Fig. 6a). However, this prediction is valid only when

$$C_0 > \sigma_{fc} \qquad (40)$$

(Fig. 4e), or

$$L_s \le \frac{C_0 t}{\tau_0}. \qquad (41)$$

Inequality (41) can be obtained from analysing Equation (36).

In contrast, if $C_0 \le \sigma_{fc}$ (Fig. 4e), two tensile fractures will occur at a distance $(C_0 t)/(2\tau_0)$ from the two ends of the brittle layer because the tensile stresses induced by

https://doi.org/10.1017/S0016756898001459 Published online by Cambridge University Press

the interbed slip in the slip regions have attained the layer tensile strength C_0. This process is referred to 'near-end fracturing'. The ultimate spacing (s) of the joints formed by this process is thus given by the following equation:

$$s=\frac{C_0}{2\tau_0}t \tag{42}$$

(Lloyd, Ferguson & Reading, 1982; Price & Cosgrove, 1990, p. 55). Equation (42) indicates that the near-end fracturing results in a linear correlation between joint spacing (s) and bed thickness (t), and shows that the joint spacing is independent of the incompetent layer thickness (d).

4. Theoretical results

For a given layer-matrix system, we first calculate the total length of the sliding interface L_s using Equation (31), and then determine the prevailing fracturing mechanism (near-end fracturing or mid-point fracturing) using inequality (41). The mid-point fracturing takes place if $L_s < C_0 t/\tau_0$, otherwise the near-end fracturing occurs. In the case where $d=t$ (Fig. 7a), the joint spacing (s) increases linearly with layer thickness (t). For the layers with the same thickness, the s value increases with the tensile strength (C_0) of the fractured layer for both the fracturing mechanisms. When the C_0 value is larger than $L_s\tau_0/t$, the fracturing mechanism is transformed from the near-end fracturing (C_0=10–40 MPa) to the mid-point fracturing ($C_0 \geq 50$ MPa). For the same t and d values, the spacing of the joints formed by mid-point fracturing is always larger than that by near-end fracturing (Fig. 7a).

Figure 7b shows the variation of joint spacing (s) with the shear strength of the bedding interface (τ_0) and bed thickness (t). In the regime of near-end fracturing, the s value decreases non-linearly with increasing τ_0 value. In the regime of mid-point fracturing, however, the s value increases first with the τ_0 value and then reaches a constant value. It is important to note that the shear strength of the bedding interface (τ_0) depends on the cohesion between beds (τ^*), the friction coefficient (μ), the normal stress on the interface (σ_n) and the pore fluid pressure (P_f):

$$\tau_0=\tau^*+\mu(\sigma_n-P_f). \tag{43}$$

The σ_n value is further affected by depth of burial (Souffaché & Angelier, 1989). Clearly, the near-end fracturing takes place preferentially at shallow and/or under high fluid pressures whereas the mid-point fracturing occurs preferentially at depth and/or under low fluid pressures.

On plots of median joint spacing (s) vs. bed thickness (t), the slope of the best-fit line is referred to as the coefficient of joint spacing (K) which is the ratio of s to t (Ladeira & Price, 1981). The K-value can be considered

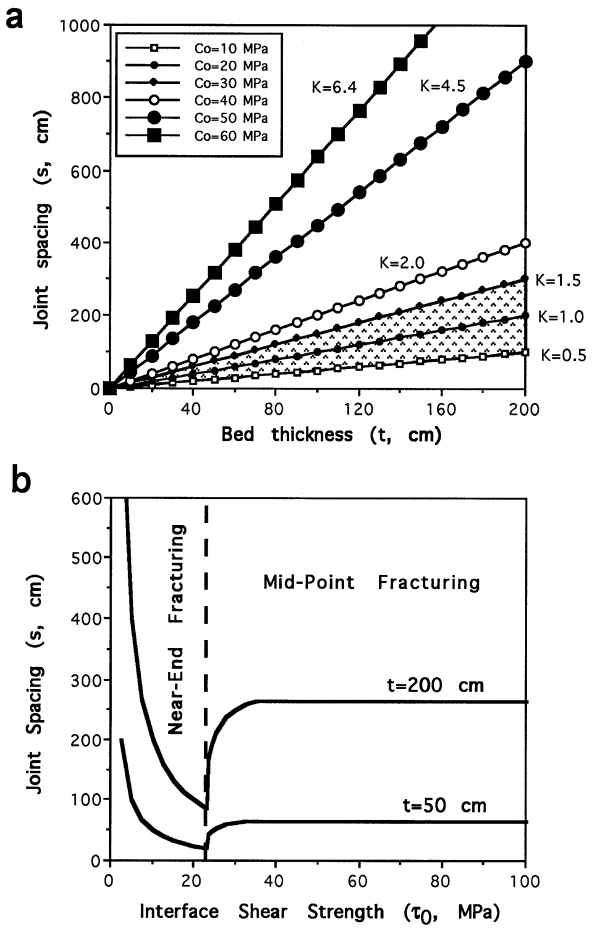


Figure 7. (a) Predicted relationship between joint spacing (s) and bed thickness (t) as a function of the tensile strength (C_0). K is the coefficient of joint spacing which is defined as the ratio of s to t. Shadow area indicates the range of K-value found in sedimentary rocks. Model parameters: E_f=58 GPa, G_m=7.74 GPa, τ_0=10 MPa, and $\varepsilon=1.12\times10^{-3}$ and $d=t$. (b) Predicted variation of joint spacing (s) with the interbed shear strength (τ_0) and bed thickness (t). Model parameters: E_f=58 GPa, G_m=7.74 GPa, C_0=20 MPa, $\varepsilon=1.12\times10^{-3}$ and $d=t$. See the text for discussion.

as an indicator of fracturing mechanism and tensile strength of the layer. As shown in Figure 7a, $K<2$ for the joints formed by the near-end fracturing while $K>4$ for the joints formed by the mid-point fracturing. In the same regime of fracturing, the K value increases with the tensile strength (Fig. 7a). As shown in Table 1, sandstones have a K-value varying from 0.60 to 1.27 with a mean value of 0.90. For limestones, the K-value varies from 0.42 to 1.34 with a mean value of 0.96. This indicates that the tensile strength of the sedimentary rocks is generally lower than 30 MPa and the joints formed most likely by near-end fracturing rather than mid-point fracturing in these rocks.

Figure 8a shows the effect of d values on the relationship between s and t. This figure is constructed using E_f=58 GPa, G_m=7.74 GPa, τ_0=10 MPa, C_0=20 MPa and $\varepsilon=1.12\times10^{-3}$. The transition from near-end frac-

https://doi.org/10.1017/S0016756898001459 Published online by Cambridge University Press

Table 1. Coefficient of joint spacing (K), defined as the slope of the median joint spacing vs. the bed thickness regression line, for typical sedimentary rocks; the K-value is an indicator for the ratio of fractured layer tensile strength to the shear strength of layer/matrix interface

Lithology	K-value	References
Sandstone	1.27	Aydan & Kawamoto (1990)
Sandstone	1.20	Price (1960)
Porcelanite & siliceous shale	0.82	Narr & Suppe (1991)
Sandstone	0.60	Angelier *et al.* (1989)
Sandstone (Alegria)	0.81	Gross (1993)
Sandstone (Gaviota)	0.79	Gross (1993)
Sandstone	0.84	This study
Chert	0.79	Narr & Suppe (1991)
Limestone	1.20	Aydan & Kawamoto (1990)
Limestone (folded)	1.34	Aydan & Kawamoto (1990)
Limestone	0.42	Angelier *et al.* (1989)
Limestone	1.35	Price (1960)
Limestone (Albian)	0.78	Huang & Angelier (1989)
Limestone (Neocomian)	0.69	Huang & Angelier (1989)
Dolostone	0.76	Narr & Suppe (1991)

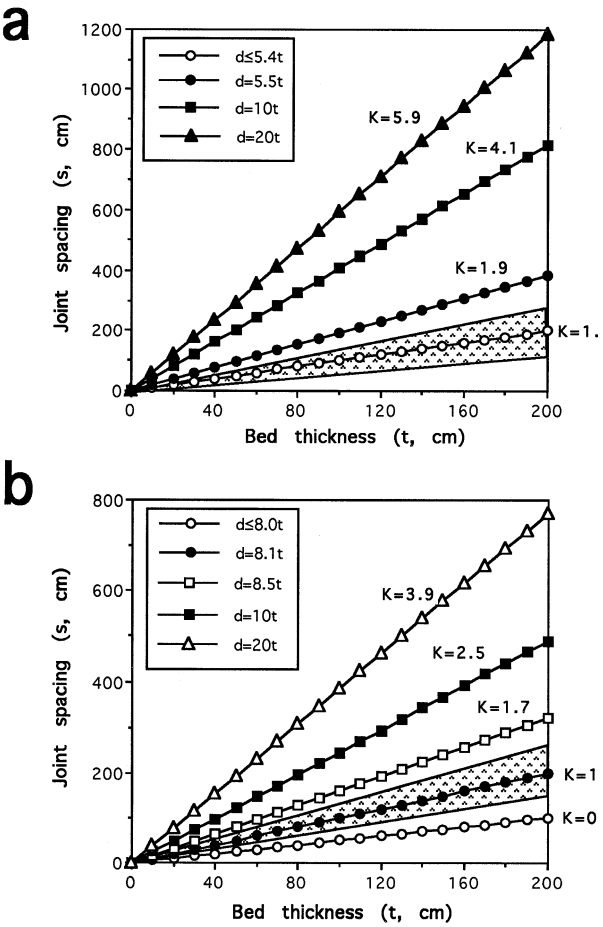


Figure 8. Predicted relationship between joint spacing (s) and bed thickness (t) as a function of the ratio of d to t. K is the coefficient of joint spacing which is defined as the ratio of s to t. Shadow area indicates the range of K-value found in sedimentary rocks. Model parameters: $E_f = 58$ GPa, $G_m = 7.74$ GPa, $\tau_0 = 10$ MPa, and $\varepsilon = 1.12 \times 10^{-3}$, $C_0 = 20$ MPa for (a) and $C_0 = 10$ MPa for (b).

turing to mid-point fracturing occurs between $d = 5.4t$ and $d = 5.5t$. In the regime of near-end fracturing ($d \leq 5.4t$), the joint spacing is independent of d value. In contrast, in the regime of mid-point fracturing, the joint spacing depends on not only the competent layer thickness (t) but also the incompetent layer thickness (d). The K-value is equal to 1 for the regime of near-end fracturing whereas $K \geq 1.9$ for the regime of mid-point fracturing. In the regime of near-end fracturing, $K = C_0/(2\tau_0)$, which is independent of the d values. Comparing Figure 8a ($C_0 = 20$ MPa) with Figure 8b ($C_0 = 10$ MPa), we noted that the critical d value for the transition from near-end fracturing to mid-point fracturing increases with decreasing the C_0 value.

5. Comparison with field data

Field data were collected from the St-Roch Formation of Lower Cambrian age in continuous exposures at Plage Victor along the Saint-Lawrence River near Saint-Jean-Port-Joli (Fig. 9) which is located 113 km northeast of Quebec city. Rocks in this area belong to the flysch sequence belt which forms the western front of the Quebec Appalachians. The regional geology of this area was given in Hubert (1967, 1969) and St-Julien (1967). According to these authors, the rocks exposed at Plage Victor can be divided into seven subunits (Fig. 9). Subunit 1 is characterized by interbedded structures of siltstones, sandstones and red and green mudstones. Subunit 2 is a slump deposit with irregular mudstone breccia, flow rolls and irregular fabrics of fold axes. Subunit 3 consists of limestone conglomerate and red and green shales. Subunit 4 is constituted of red and green shales with laminated calcareous siltstones. Subunit 5 is characterized by green and gray mudstones interbedded with thick laminated limestones and siltstones. Subunit 6 consists of interbedded limestones and gray and green mudstones. Subunit 7 consists of red and green mudstones and thin beds of sandstones. Lithology and thickness of the sandstone beds are persistent laterally. Our joint data were measured mainly from subunits 1 and 7.

The tectonic structures of the area are characterized by northeast–southwest trending folds and reverse faults which formed during the Appalachian compression. In the study area (900×300 m^2), tectonic strain is fairly homogeneous except near the faults (Fig. 9). Joints are generally confined to the hard sandstone, siltstone and limestone layers while the soft shale and mudstone layers remain non-jointed (Fig. 10). This has been interpreted by Becker & Gross (1996) as indicating that the stress intensity at joint tips reaches a critical value within the competent layers while it is below this critical value within the incompetent layers. The joints are approximately planar fractures with

https://doi.org/10.1017/S0016756898001459 Published online by Cambridge University Press

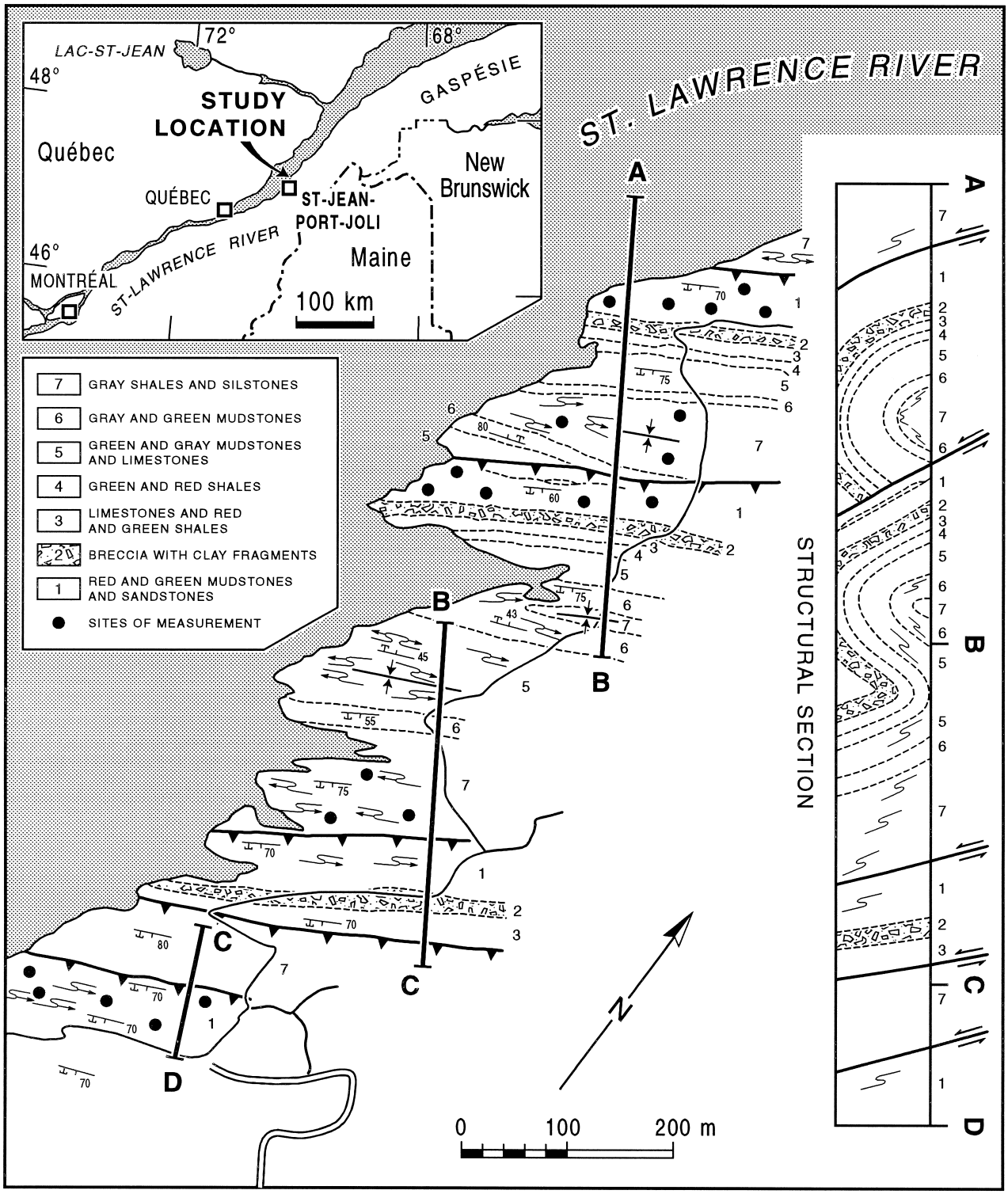


Figure 9. Geological map of Plage Victor along the Saint-Lawrence River near Saint-Jean-Port-Joli, Quebec. Modified from Hubert (1967, 1969). The joint data were measured mainly from subunits 1 and 7.

little or no offset parallel to the fracture plane, and thus extension fractures ('mode I' cracks of fracture mechanics) which formed as the result of extensional strain normal to the plane of fracture (Pollard & Aydin, 1988). Most of the joints except some of those within the fault zones are entirely barren, that is, free of calcite or quartz vein infilling (Fig. 10). The only evidence of interbed slip we have found is that the mudstone or shale is less sheared at the centre of the layer than near the contacts with sandstone or limestone. This is not surprising to us because the amount of displacement across the layer/matrix interfaces

https://doi.org/10.1017/S0016756898001459 Published online by Cambridge University Press

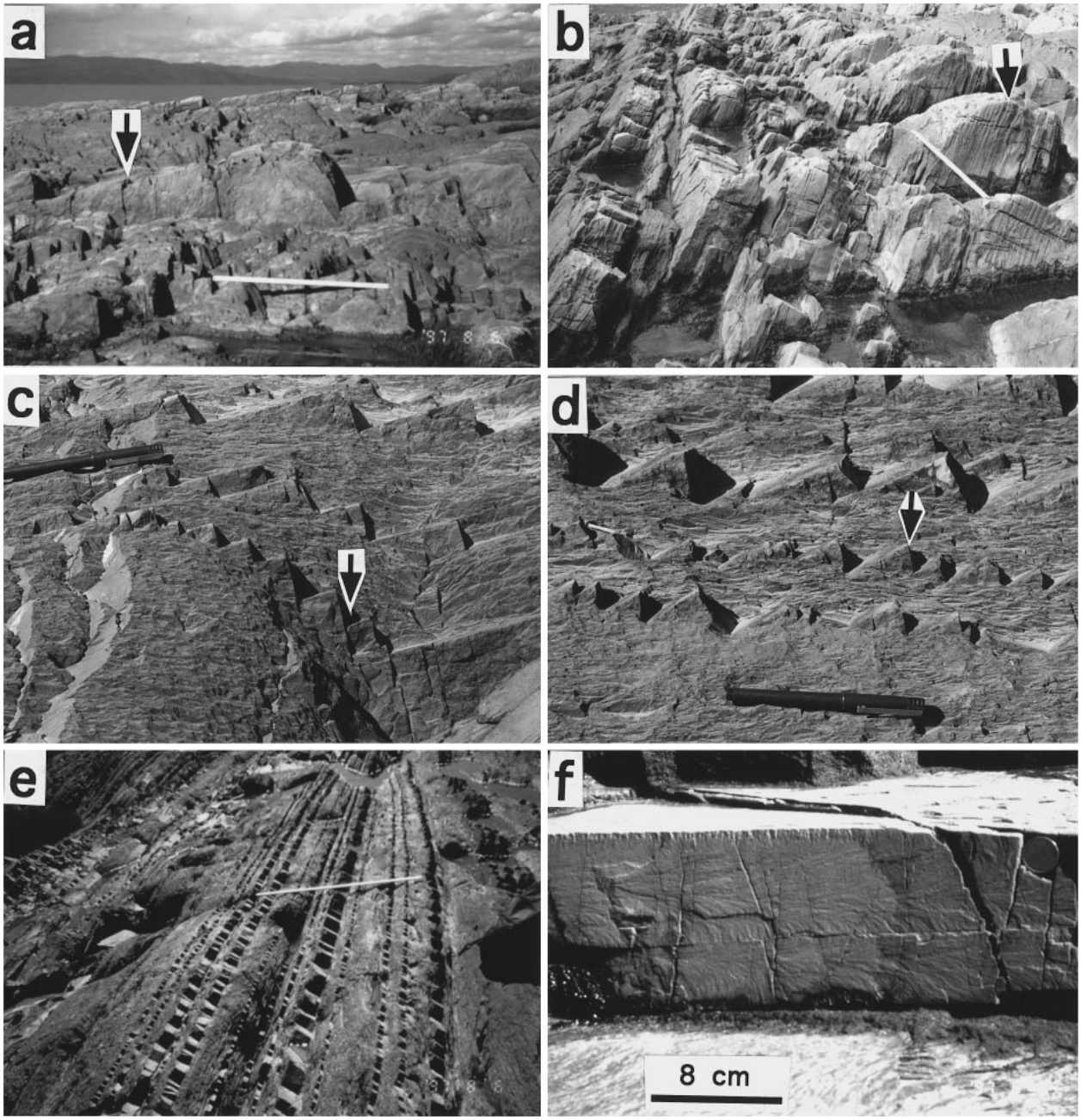


Figure 10. Photographs of the interbedded sedimentary rocks at Plage Victor along the Saint-Laurent River near Saint-Jean-Port-Joli, Quebec. Jointing layers are competent sandstone in (a) and (c–f) and limestone in (b) while non-jointing layers are incompetent mudstone or shale. The systematic set of steeply dipping joints (indicated by arrow) was chosen for the present study. Note that the joint spacing in thicker sandstone layers is regularly greater than in thinner beds. (f) Joint plane in a fine-grained sandstone showing a plumose structure diverging from a point indicating propagation away from a point. Length of ruler in (a, b, e): 1.0 m. Length of pen in (c, d): 0.14 m.

involved in the formation of extensional joints is very small and certainly insufficient to form lineated fiber sheets along the bedding planes.

There are two orthogonal sets of joints: one strikes about 325–340° and dips between 65° and 85°, and the other trends about 140–155° and dips about 10–30°. The first set is predominant, systematic and normal to the fold axes and is considered to have been formed due to the folding-related regional tectonic extension. The second set is abutting and intersecting the predominant set of joints and can be interpreted as cross joints (Hancock, 1985; Hancock *et al.* 1987; Gross, 1993). As pointed out recently by Caputo (1995), the cross joints appear to be locally younger than the systematic joints, but from a geological time-scale perspective both sets are coeval and formed during a continuous fracturing process. Only the predominant set was measured in the field because the joints are so favourably oriented with respect to horizontal outcrop exposure that the measurements were easily carried out.

https://doi.org/10.1017/S0016756898001459 Published online by Cambridge University Press

Joint spacing, which is defined as the perpendicular distance between adjacent joints belonging to the same set, in thick beds is commonly greater than in thin beds, as shown in Figure 10a–e. Jointed layers satisfying the following conditions were selected for measurement: (1) the layers display uniform lithology and thickness along its length; (2) the layers are not disturbed by faults because joints are extremely closely spaced in the vicinity of faults and were formed by the shearing along the faults rather than by layer-parallel extensional strain (Becker & Gross, 1996); (3) the layers are bounded by two incompetent layers nearly identical in thickness; and (4) in a single layer, there should be a sufficient number of parallel joints (at least 50 for beds thinner than 1.0 m or 25 for beds thicker than 1.0 m) whose spacing could be measured on a continuous outcrop. In total, 87 sandstone layers were measured.

In the bedding planes, joint length is much greater than spacing (Fig. 10c, f), indicating that the joints are 'well developed' according to the laboratory-derived classification of Wu & Pollard (1995). Plume structures (Fig. 10f) and rib marks on joint surfaces in uniform fine-grained siltstones and limestones indicate that the joints initiated and propagated away from point defects such as nodules, pebbles, pores, and minerals (Price, 1966; Syme-Gash, 1971; Bahat & Engelder, 1984). It may be reasonable to assume that such defects are randomly distributed in the rocks.

The joint spacings belonging to the systematic set along an individual bed with a uniform thickness generally display an appearance of normal distribution (Fig. 11a–d) and occasionally positively skewed frequency distribution (Fig. 11e–f). The normal distribution is symmetric and the median, mean and mode are nearly identical (Fig. 11a–d). For the positively skewed distribution, however, the median is significantly less than the mean but larger than the mode (Fig. 11e–f). Similar skewed distributions have been described as gamma distributions (Huang & Angelier, 1989; Gross, 1993) or log-normal distributions (Sen & Kazi, 1984; Narr & Suppe, 1991; Rives *et al.* 1992; Becker & Gross, 1996). Huang & Angelier (1989) suggest that the skewed distributions are due to censuring of the minute joints, which do not cut completely the competent layer, during measurements. Their suggestion is based on a fact that there are several different orders of spacing of joints in rocks and only the larger orders are visible as joints. Narr & Suppe (1991) and Becker & Gross (1996) propose that such distributions are a direct consequence of the stress reduction shadow, which inhibits formation of new joints in the vicinity of existing joints. Rives *et al.* (1992) suggest that joint set development is controlled by the spatial distribution of initiation points, the size of the interaction zones, the initiation and propagation criteria of the joint set, and the stage of evolution. The evolution from a negative exponential to a normal distribution through a log-normal distribution corresponds to an increase in degree of fracture saturation and, by inference, in extension strain. According to Rives *et al.* (1992), the normal distribution of joint spacing indicates that most jointed layers we measure today are quasi-saturated. Therefore, the relationship between joint spacing and bed thickness may provide meaningful insights about the material properties of the rocks because the spacing is not sensitive to the applied strain at the stage of fracture saturation (Wu & Pollard, 1995).

Figure 12 shows plots of median joint spacing vs. layer thickness for 87 sandstone beds. Each point in Figure 12 is the median spacing of 26–300 measurements. The best-fit line for these data is a straight line with a slope equal to 0.84 although the data are more scattered for $t > 20$ cm than $t < 20$ cm. It is noteworthy to observe an independence of the s–t relationship on the sampling sites which occupy different structural positions in the study area (Fig. 9). The independence also indicates a state of fracture saturation.

The mathematical calculation of the theoretical joint spacing in the sandstone layers requires the following input data: (1) the Young's modulus (E_f) and tensile strength (C_0) of sandstone; (2) the shear modulus of shale or mudstone (G_m); (3) the shear strength of the sandstone/shale (or mudstone) interface (τ_0); (4) the fracture saturation strain (ε); (5) the t and d values collected in the field (Fig. 13). In the present study, $E_f = 58$ GPa, which is obtained by averaging all the Young's moduli calculated from P-wave velocities and densities of sandstones at 100 MPa (Christensen, 1989). For the shale, we assume that $G_m = 7.74$ GPa (Gross *et al.* 1995; Fischer *et al.* 1995). The corresponding elastic contrast between sandstone and shale $E_f/E_m = 3$ if the Poisson's ratio of the shale $\upsilon_m = 0.25$. The shear strength of the bedding interface (τ_0) varies with the cohesion between beds (τ^*), the friction coefficient (μ), the normal stress on the interface (σ_n) and the pore fluid pressure (P_f). The fracture saturation strain is assumed as $\varepsilon = 1.12 \times 10^{-3}$. It should be pointed out that the calculated results on joint spacing depend mainly on the values of E_f/E_m and C_0/τ_0 rather than the absolute values of E_f, E_m, τ_0 and C_0.

Our modelling for each jointing layer proceeds in the following order: (1) determining the length of the sliding interface L_s using Equation (31); (2) identifying whether the prevailing fracturing mechanism is the mid-point fracturing (if $L_s < C_0 t/\tau_0$) or the near-end fracturing (if $L_s \geq C_0 t/\tau_0$), using inequality (41); and (3) calculating the theoretical joint spacing using Equation (38) for the mid-point fracturing or using Equation (42) for the near-end fracturing.

Figure 14 summarizes the calculated results for 87 sandstone layers whose t, d and s values have been measured in the field. Effects of C_0 on the s–t relationship can be analysed in detail from either Figure 14a or Figure 14b. For $\tau_0 = 10$ MPa, the sandstone layers

https://doi.org/10.1017/S0016756898001459 Published online by Cambridge University Press

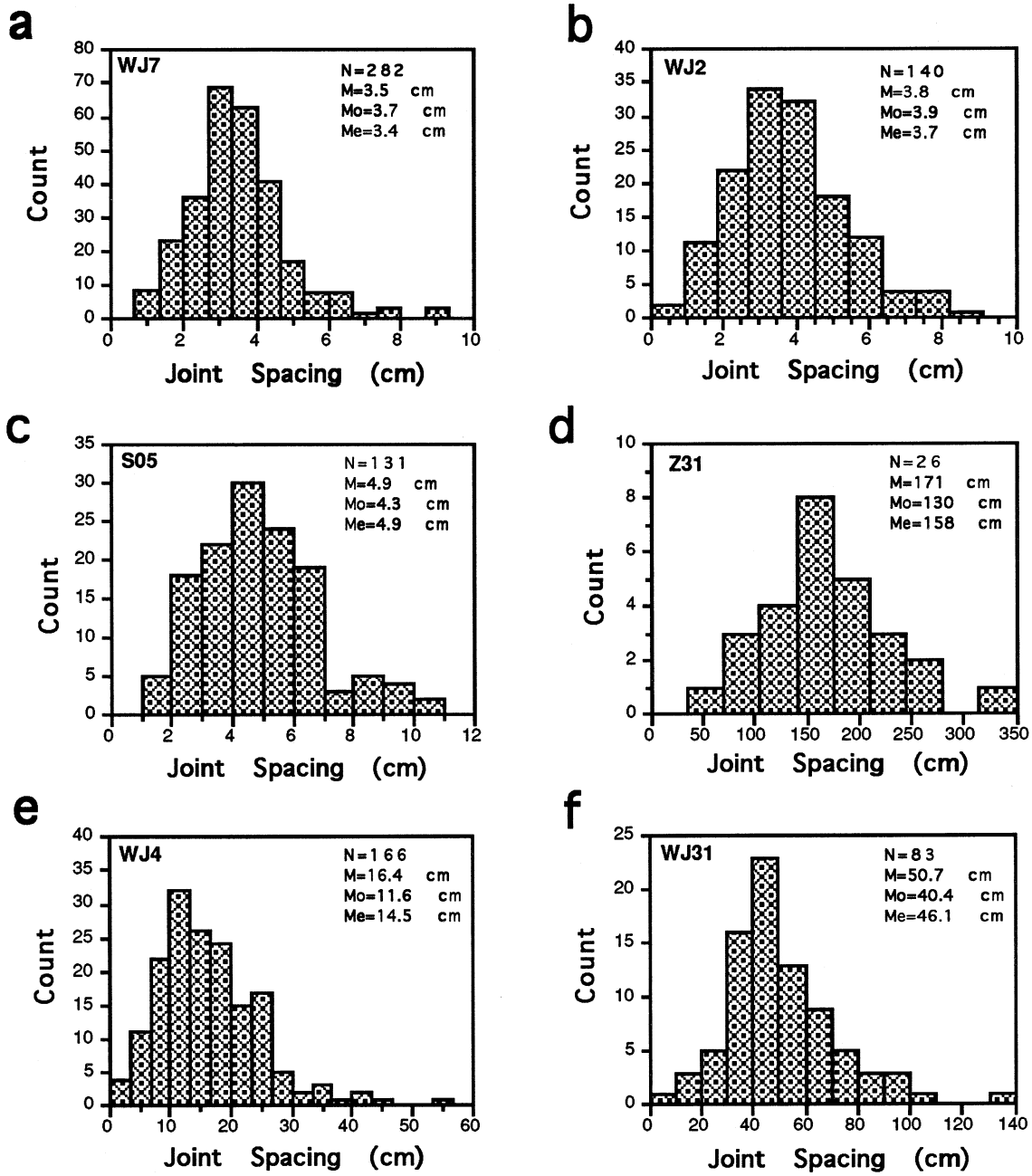


Figure 11. Histograms for joint spacing values measured in six typical sandstone layers at Plage Victor in the Saint-Jean-Port-Joli area of the Quebec Appalachians. N, the number of measurements; M, the arithmetic mean; Mo, the mode (the most frequently occurring value in the distribution); Me, the median (the fiftieth percentile in the distribution).

with $C_0 \leq 30$ MPa are dominated by the near-end fracturing process while the layers with $C_0 = 50$ MPa are jointed by both the near-end fracturing and mid-point fracturing (Fig. 14a). By comparing Figure 14a with Figure 14b, one can find that the critical value of for the transition from the near-end fracturing to the mid-point fracturing decreases with increasing τ_0 value. For $\tau_0 = 20$ MPa (Fig. 14b), the sandstone layers with $C_0 > 30$ MPa are dominantly jointed by the mid-point fracturing process. It is interesting to note that the coefficient of joint spacing (K-value) decreases with increasing τ_0 value in the regime of the near-end fracturing (also see Fig. 7b). Because the τ_0 value is mainly affected by depth of burial and pore fluid pressure, the K-value should increase with increasing the pore fluid pressure and decrease with increasing depth of burial.

In the regime of near-end fracturing, the predicted joint spacing increases linearly with sandstone layer thickness (t) and is independent of shale or mudstone thickness (d). In the regime of mid-point fracturing, however, the predicted joint spacing depends on both t and d values and thus the s–t relationship becomes complex (Fig. 14).

Under the specific model conditions of Figure 14a, a good agreement between the calculated and measured relationships between s and t is found using

https://doi.org/10.1017/S0016756898001459 Published online by Cambridge University Press

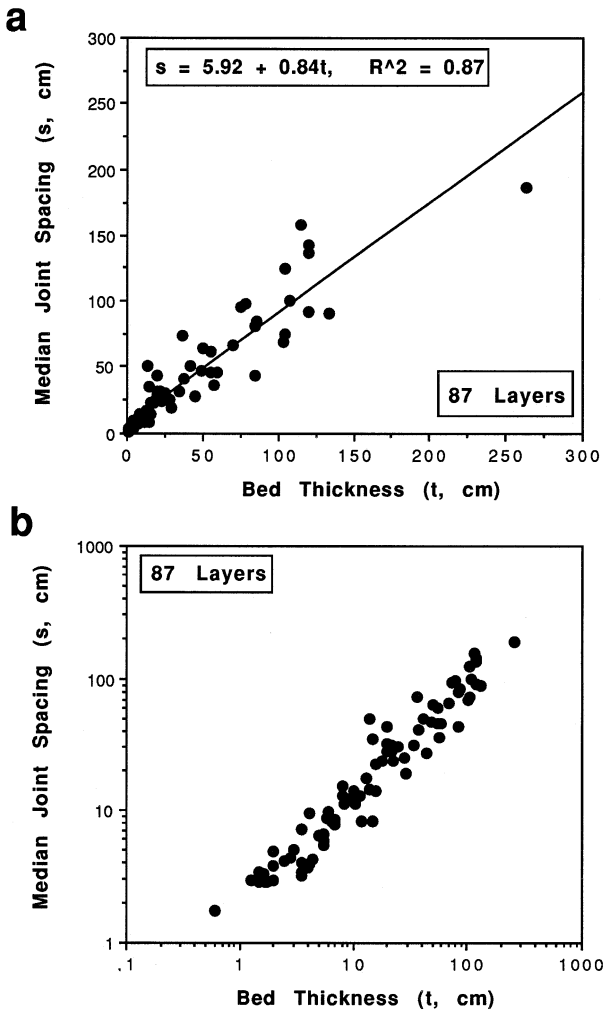


Figure 12. Plots of median joint spacing (s) vs. bed thickness (t) of sandstone, measured from Plage Victor in the Saint-Jean-Port-Joli area of the Quebec Appalachians. Data from 87 layers. (a) The data are represented in a linear scale so that the linear relationship between joint spacing and bed thickness may readily be seen. (b) The data are represented in a logarithmic scale in order to obviate the problem relating to the unresolvable data near the origin.

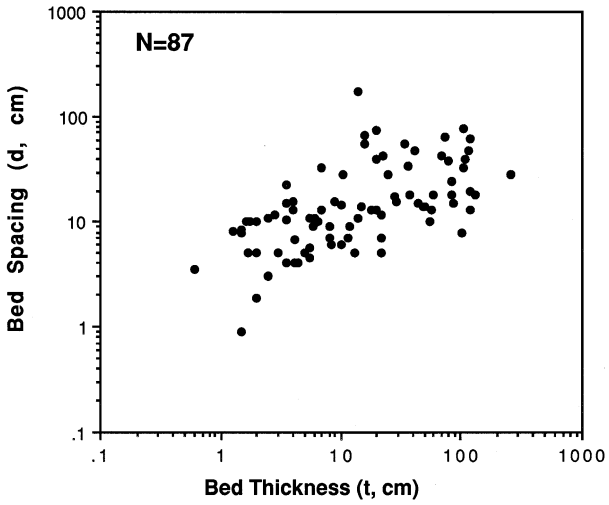


Figure 13. Thicknesses of the sandstone and its bounding shale or mudstone layers at 87 study sites from Plage Victor in the Saint-Jean-Port-Joli area of the Quebec Appalachians.

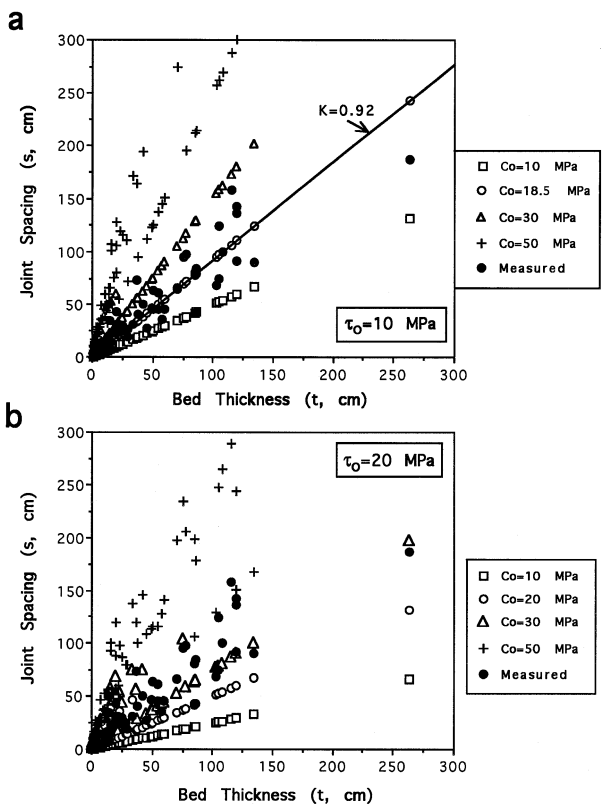


Figure 14. Comparison between the calculated and measured results. Model parameters: E_f=58 GPa, G_m=7.74 GPa, $\varepsilon=1.12\times10^{-3}$ and measured t and d data in Figure 13. (a) τ_0=10 MPa and (b) τ_0=20 MPa. A good agreement between the measured and calculated s–t relationship is found using τ_0=10 MPa and C_0=18.5 MPa. See the text for discussion.

C_0=18.5 MPa. The wide dispersion of the measured data with respect to the calculated data is thought to be due to the fact that the natural rock layers are not uniform in mechanical properties such as E_f and C_0 or in flaw size and distribution (Jaeger, 1969; Adams & Sines, 1978). In addition, the properties of rock layers at different outcrops may be slightly different due to differences in composition and microstructure. It is reasonable to assume the mean tensile strength of the sandstone and the sandstone/shale interfacial shear strength in the study area as ~18.5 MPa and ~10 MPa, respectively. It is particularly important to note that the s–t relationship measured from the Plage Victor in the Saint-Jean-Port-Joli area is mainly located in the regime of the near-end fracturing rather than in that of the mid-point fracturing. In other words, the above analysis of the relationship between the joint spacing (s) and bed thicknesses (t and d) may allow a distinction to be made between the proposed modes of fracturing.

https://doi.org/10.1017/S0016756898001459 Published online by Cambridge University Press

6. Limitations of the model

It should be kept in mind that our shear-lag model deals with the distribution of joints in sedimentary rocks comprising alternating competent and incompetent beds. Apparently, the model cannot be applied to massive rock units or igneous intrusions where joints were formed by mechanisms which are different from the stress transfer discussed above. Effects of residual stresses, bending, cooling and unloading should play a major role in building up tensile stresses for formation of fractures in the massive rocks.

The relationship between joint spacing and bed thickness depends on the actual mode of the shear stress decay in the matrix. For simplicity in the mathematical treatment, we assumed a linear decay for the shear stress distribution in the matrix although a non-linear mode may be more realistic (Fischer *et al.* 1992; Ji & Saruwatari, in press). The actual mode should be studied by well-designed experiments in future.

In the present study, we assumed that the competent layer has a unique tensile strength whereas in a natural sedimentary bed, a fairly wide distribution of strengths is expected (Narr & Suppe, 1991; Rives *et al.* 1992) along the layer due to the random nature of defects (e.g. nodules, pebbles, pores, minerals and fossils). We thus consider this work as a preliminary step for a more complex probabilistic modelling (Pascal *et al.* 1997) on the distribution of joints.

The principal limitation to the model presented in this paper is the assumption that the two incompetent layers bounding the jointed layer are of equal thickness. This arises from the simple form for the equation of mechanical equilibrium (Eq. (24)). This assumption is also included in the previous models (Price, 1966; Hobbs, 1967; Narr & Suppe, 1991; Gross *et al.* 1995; Fischer *et al.* 1995; Ji & Saruwatari, in press). In order to remove this limitation, a complex unit-cell must be used and this cannot be treated with the present analytic solution. Nevertheless the analysis, we believe, has important value for the bedded sedimentary rocks with nearly identical jointed layer spacings. A rigorous elastic analysis is possible at present by only numerical methods, but it may be too tedious to employ for each actual layer measured in the field.

The present model is two-dimensional and implicitly assumes that joints are infinite in the third direction. Thus, the interaction between joints in this direction is ignored. Effects of the interaction on the frequency distribution of joint spacing have been discussed by Rives *et al*. (1992) and Wu & Pollard (1995).

The general trend of the field measurement results can be predicted by the model. It should be emphasized, however, that the prediction is based on the assumptions inherent in the model and on the selection of material constants (E_f, G_m, τ_0, C_0) and fracture saturation strain (ε) for the rocks. We believe that the theoretical model will be useful for analysing the relationship between joint spacing and bed thickness.

7. Conclusions

The effects of interbed slip have been ignored in all the previous mechanical analyses of joint spacing as a function of bed thickness in sedimentary rocks (Price, 1966; Hobbs, 1967; Sowers, 1973; Ladeira & Price, 1981; Pollard & Segall, 1987; Souffaché & Angelier, 1989; Mandal, Deb & Khan, 1994; Fischer *et al.* 1995; Gross *et al.* 1995). In the present paper, we have developed a new mechanical model to include the effects of interbed slip on the relationship between joint spacing and jointed layer thickness.

Our model shows that the interbed slip can result in two different fracturing processes: near-end fracturing and mid-point fracturing. The near-end fracturing occurs in the layers with smaller tensile fracture strength ($C_0 \leq 30$ MPa) and/or smaller interbed shear strength ($\tau_0 < 20$ MPa) while the mid-point fracturing occurs in those layers with larger C_0 (≥ 50 MPa) and τ_0 (> 30 MPa) values. For the rocks with moderate tensile fracture strength ($30 < C_0 < 50$ MPa) and interbed shear strength ($20 < \tau_0 < 30$ MPa) values, the near-end fracturing and mid-point fracturing take place preferentially in the thicker and thinner brittle layers, respectively.

In the regime of near-end fracturing, the correlation between joint spacing and bed thickness is linear and independent of the incompetent layer thickness. In the regime of mid-point fracturing, however, the relationship between joint spacing and bed thickness can be either linear or non-linear, depending on the variations of the incompetent layer thickness (Ji & Saruwatari, in press).

The coefficient of joint spacing (K) is defined by the slope of the regression line to express the ratio of median joint spacing to bed thickness. The K-values measured from typical sedimentary beds such as sandstones (Price, 1960; Huang & Angelier, 1989; Angelier *et al.* 1989; Gross, 1993; Aydan & Kawamoto, 1990; Narr & Suppe, 1991) varies from 0.60 to 1.27 with a mean value of 0.90. This indicates that the tensile strength of sandstone (C_0) is generally lower than 30 MPa and the interbed shear strength (τ_0) is about 10 MPa. Under these conditions, the joints are formed most likely by the near-end fracturing rather than by the mid-point fracturing in these rocks. Thus, the K-value can be considered as an indicator of $C_0/(2\tau_0)$ ratio.

Acknowledgements. We are indebted to Kathie St-Amand and Kazuko Saruwatari for their assistance in the field, Michel Demidoff for drawing Figures 2 and 9, and Kazuko Saruwatari for drawing Figures 4 and 11. Particular thanks are due to Paul Hancock, Richard Lisle and J. Holland for critical remarks and constructive comments. This study was supported by research grants from the NSERC of Canada to S. Ji. This is LITHOPROBE contribution no. 933.

https://doi.org/10.1017/S0016756898001459 Published online by Cambridge University Press

References

ADAMS, M. & SINES, G. 1978. Crack extension from flaws in a brittle material subjected to compression. *Tectonophysics* **49**, 97–118.

ANGELIER, J., SOUFFACHÉ, B., BARRIER, E., BERGERAT, F., BOUAZIZ, S., BOUROZ, C., CREUZOT, G., OUALI, J. & TRICART, P. 1989. Distribution de joints de tension dans un banc rocheux: loi théorique et. *Comptes Rendus de l'Academie des Sciences* **309**, 2119–25.

AYDAN, O. & KAWAMOTO, T. 1990. Discontinuities and their effect on rock mass. In *Rock Joints* (eds N. Barton and O. Stephansson), pp. 149–56. Rotterdam: Balkema.

BAHAT, D. & ENGELDER, T. 1984. Surface morphology on cross-fold joints of the Appalachian plateau, New York and Pennsylvania. *Tectonophysics* **104**, 299–313.

BARTON, C. C. & LARSEN, E. 1985. Fractal geometry of two-dimensional fracture networks at Yucca Mountain, southwestern Nevada. In *Proceeding of the International Symposium on Fundamentals of Rock Joints*, pp. 77–84. Björkliden, Sweden.

BECKER, A. & GROSS, M. R. 1996. Mechanism for joint saturation in mechanically layered rocks – an example from southern Israel. *Tectonophysics* **257**, 223–37.

BEAR, J., TSANG, C.-F. & DE MARSILY, G. 1993. *Flow and Contaminant Transport in Fractured Rock*. San Diego, California: Academic Press.

BOGDANOV, A. A. 1947. The intensity of cleavage as related to the thickness of beds. *Soviet Geology* **16** (in Russian).

CAPUTO, R. 1995. Evolution of orthogonal sets of coeval extension joints. *Terra Nova* **7**, 479–90.

CHRISTENSEN, N. I. 1989. Seismic velocities. In *Practical Handbook of Physical Properties of Rocks and Minerals* (ed. R. S. Carmichael), pp. 429–546. Boca Raton, Florida: CRC Press.

COX, H. L. 1952. The elasticity and strength of paper and other fibrous materials. *British Journal of Applied Physics* **3**, 72–9.

DELOULE, E. & TURCOTTE, D. L. 1989. The flow of hot brines in cracks and the formation of ore deposits. *Economical Geology* **84**, 2217–25.

FISCHER, M. P., GROSS, M. R., ENGELDER, T. & GREENFIELD, R. J. 1995. Finite-element analysis of the stress distribution around a pressurized crack in a layered elastic medium: implications for the spacing of fluid-driven joints in bedded sedimentary rock. *Tectonophysics* **247**, 49–64.

GROSS, M. R. 1993. The origin and spacing of cross joints: examples from the Monterey Formation, Santa Barbara Coastline, California. *Journal of Structural Geology* **15**, 737–51.

GROSS, M. R., FISCHER, M. P., ENGELDER, T. & GREENFIELD, R. J. 1995. Factors controlling joint spacing in interbedded sedimentary rocks: integrating numerical models with field observations from the Monterey Formation, USA. In *Fractography: Fracture Topography as a Tool in Fracture Mechanics and Stress Analysis* (ed. M. S. Ameen), pp. 215–53. Geological Society, London, Special Publication no. 92.

HANCOCK, P. L. 1985. Brittle microtectonics: principles and practice. *Journal of Structural Geology* **7**, 435–57.

HANCOCK, P. L., AL-KADHI, A., BARKA, A. A. & BEVAN, T. G. 1987. Aspects of analyzing brittle structures. *Annales Tectonicae* **1**, 5–19.

HOBBS, D. W. 1967. The formation of tension joints in sedimentary rocks: an explanation. *Geological Magazine* **104**, 550–6.

HUANG, Q. & ANGELIER, J. 1989. Fracture spacing and its relation to bed thickness. *Geological Magazine* **126**, 355–62.

HUBERT, C. 1967. Tectonics of part of the Sillery Formation in the Chaudiere-Matapedia segment of the Quebec Appalachians. *Royal Society of Canada Special Publication* **10**, 33–41.

HUBERT, C. 1969. *Guidebook-Flysch Sedimentology in the Appalachians*. The Geological Association of Canada and The Mineralogical Association of Canada, Montreal.

JAEGER, J. C. 1969. *Elasticity, Fracture and Flow with Engineering and Geological Applications*. Methun & Co. Ltd. and Science Paperbacks. New York: John Wiley & Sons, Inc.

JI, S. & SARUWATARI, K. In press. A revised model for the relationship between joint spacing and layer thickness. *Journal of Structural Geology.*

JI, S. & ZHAO, P. 1993. Location of tensile fracture within rigid-brittle inclusions in ductile flowing matrix. *Tectonophysics* **220**, 23–31.

JI, S. & ZHAO, P. 1994. Strength of two-phase rocks: a model based on fiber-loading theory. *Journal of Structural Geology* **16**, 253–62.

KELLY, A. & MACMILLAN, N. H. 1986. *Strong solids*. Oxford: Oxford Science Publications.

KIRILLOVA, I. V. 1949. Some problems of the mechanics of folding. *Trans. Geofian* **6** (in Russian).

KREYSZIG, E. 1993. *Advanced Engineering Mathematics.* New York: John Wiley & Sons, Inc. 929 pp.

LACHENBRUCH, A. H. 1961. Depth and spacing of tension cracks. *Journal of Geophysical Research* **66**, 4273–92.

LADEIRA, F. L. & PRICE, N. J. 1981. Relationship between fracture spacing and bed thickness. *Journal of Structural Geology* **3**, 179–83.

LLOYD, G. E., FERGUSON, C. C. & READING, K. 1982. A stress-transfer model for the development of extension fracture boudinage. *Journal of Structural Geology* **4**, 355–72.

LORENZ, J. C., TEUFEL, L. W. & WARPINSKI, N. R. 1991. Regional fractures I: a mechanism for the formation of regional fractures at depth in flat-lying reservoirs. *The American Association of Petroleum Geologists Bulletin* **75**, 1714–37.

MANDAL, N., DEB, S. K. & KHAN, D. 1994. Evidence for a non-linear relationship between fracture spacing and layer thickness. *Journal of Structural Geology* **16**, 1275–81.

MASUDA, T. & KURIYAMA, M. 1988. Successive "mid-point" fracturing during microboudinage: an estimate of the stress-strain relation during a natural deformation. *Tectonophysics* **147**, 171–7.

MASTELLA, L. 1972. Interdependence of joint density and the thickness of layers in the Podhale Flysch. *Bulletin de l'Academie des Sciences de Pologne* **20**, 187–96.

MCQUILLAN, H. 1973. Small-scale fracture density in Asmari formation of southwest Iran and its relation to bed thickness and structural setting. *The American Association of Petroleum Geologists Bulletin* **57**, 2367–85.

NARDONE, V. C. & PREWO, K. M. 1986. On the strength of discontinuous silicon carbide reinforced aluminum composites. *Scripta Metallurgica et Materialia* **20**, 43–8.

NARR, W. & SUPPE, J. 1991. Joint spacing in sedimentary rocks. *Journal of Structural Geology* **13**, 1037–48.

https://doi.org/10.1017/S0016756898001459 Published online by Cambridge University Press

NORRIS, D. K. 1966. The mesoscopic fabric of rock masses about some Canadian coal mines. *Proceeding of the Congress of International Society of Rock Mechanics, Lisbon, Portugal* **1**, 191–8.

NOVIKOVA, A. C. 1947. The intensity of cleavage as related to the thickness of the bed. *Soviet Geology* **16** (in Russian).

OHSAWA, T., NAKAYANA, A., MIWA, M. & HASEGAWA, A. 1978. Temperature dependence of critical fiber length for glass fiber reinforced thermosetting resins. *Journal of Applied Polymer Science* **22**, 3203–12.

PASCAL, C., ANGELIER, J., CACAS, M.-C. & HANCOCK, P. L. 1997. Distribution of joints: probabilistic modeling and case study near Cardiff (Wales, U.K.). *Journal of Structural Geology* **19**, 1273–84.

PIGGOTT, M. R. 1980. *Load Bearing Fibre Composites*. Oxford: Pergamon Press.

POLLARD, D. D. & AYDIN, A. 1988. Progress in understanding jointing over the past century. *Geological Society of America Bulletin* **100**, 1181–1204.

POLLARD, D. D. & SEGALL, P. 1987. Theoretical displacements and stresses near fractures in rocks, with applications to faults, joints, veins, dikes, and solution surfaces. In *Fracture Mechanics of Rock* (ed. B. K. Atkinson), pp. 277–349. London: Academic Press.

PRICE, N. J. 1966. *Fault and joint development in brittle and semi-brittle rock*. Oxford: Pergamon Press.

PRICE, N. J. & COSGROVE, J. M. 1990. *Analysis of Geological Structures*. Cambridge: Cambridge University Press.

RAMBERG, H. 1955. Natural and experimental boudinage and pinch-and-swell structures. *Journal of Geology* **63**, 512–26.

REYNOLDS, S. J. & LISTER, G. S. 1987. Structural aspects of fluid-rock interactions in detachment zones. *Geology* **15**, 362–6.

RIVES, T., RAZACK, M., PETIT, J.-P. & RAWNSLEY, K. D. 1992. Joint spacing: analogue and numerical simulations. *Journal of Structural Geology* **14**, 925–37.

SEN, Z. & KAZI, A. 1984. Discontinuity spacing and RQD estimates from finite length scanlines. *International Journal of Rock Mechanics and Mining Sciences and Geomechanics Abstracts* **21**, 203–12.

SOUFFACHÉ, B. & ANGELIER, J. 1989. Distribution de joints de tension dans un banc rocheux: principe d'une modélisation énergétique. *Comptes Rendus de l'Academie des Sciences* **308**, Série II, 1385–90.

SOWERS, G. M. 1973. Theory of spacing of extension fracture. *Engineering Geology Case Histories* **9**, 27–53.

ST-JULIEN, P. 1967. Tectonics of part of the Appalachian region of southeastern Quebec. *Royal Society of Canada Special Publications* **10**, 41–7.

SYME-GASH, P. J. 1971. A study of surface features relating to brittle and semibrittle fracture. *Tectonophysics* **12**, 349–91.

THUNVIK, R. & BRAESTER, C. 1990. Gas migration in discrete fracture networks. *Water Resource Research* **26**, 2425–34.

WU, H. & POLLARD, D. D. 1992. Propagation of a set of opening-mode fractures in layered brittle materials under uniaxial strain cycling. *Journal of Geophysical Research* **97**, 3381–96.

WU, H. & POLLARD, D. D. 1995. An experimental study of the relationship between joint spacing and layer thickness. *Journal of Structural Geology* **17**, 887–905.

ZHAO, P. & JI, S. 1992. Comment on "Strengthening behavior of particulate reinforced MMCs" by Y. Wu & E. J. Lavernia, and "On the strength of discontinuous silicon carbide reinforced aluminum composites" by V. C. Nardone & K. M. Prewo. *Scripta Metallurgica et Materialia* **27**, 1443.

ZHAO, P. & JI, S. 1997. Refinements of shear-lag model and its applications. *Tectonophysics* **279**, 37–53.

https://doi.org/10.1017/S0016756898001459 Published online by Cambridge University Press